Anisotropic semivortices in dipolar spinor condensates controlled by Zeeman splitting

Bingjin Liao, Shoubo Li, Chunqing Huang, Zhihuan Luo, Wei Pang, Haishu Tan, Boris A. Malomed, and Yongyao Li

Phys. Rev. A **96**, 043613 — Published 16 October 2017

DOI: 10.1103/PhysRevA.96.043613

Anisotropic semi-vortices in dipolar spinor condensates controlled by Zeeman splitting

Bingjin Liao[1], Shoubo Li[1], Chunqing Huang[1], Zhihuan Luo[2], Wei Pang[3], Haishu Tan[1], Boris A. Malomed[4,5,1], and Yongyao Li[1*]

[1] *School of Physics and Optoelectronic Engineering, Foshan University, Foshan 528000, China*
[2] *College of Electronic Engineering, South China Agricultural University, Guangzhou 510642, China*
[3] *Department of Experiment Teaching, Guangdong University of Technology, Guangzhou 510006, China*
[4] *Department of Physical Electronics, School of Electrical Engineering, Faculty of Engineering, Tel Aviv University, Tel Aviv 69978, Israel.*
[5] *Laboratory of Nonlinear-Optical Informatics, ITMO University, St. Petersburg 197101, Russia*

Spatially anisotropic solitary vortices, i.e., bright anisotropic vortex soliton (AVSs), supported by anisotropic dipole-dipole interactions, were recently predicted in spin-orbit-coupled binary Bose-Einstein condensates (BECs), in the form of two-dimensional semi-vortices (complexes built of zero-vorticity and vortical components). We demonstrate that the shape of the AVSs – horizontal or vertical, with respect to the in-plane polarization of the atomic dipole moments in the underlying BEC – may be effectively controlled by strength Ω of the Zeeman splitting (ZS). A transition from the horizontal to vertical shape with the increase of Ω is found numerically and explained analytically. At the transition point, the AVS assumes the shape of an elliptical ring. Mobility of horizontal AVSs is studied too, with a conclusion that, with the increase of Ω, their negative effective mass changes the sign into positive via a point at which the effective mass diverges. Lastly, we report a new species of *inverted* AVSs, with the zero-vorticity and vortex component placed in lower- and higher-energy components, as defined by the ZS. They are excited states, with respect to the ground states provided by the usual AVSs. Quite surprisingly, inverted AVSs are *stable* in a large parameter region.

PACS numbers: 42.65.Tg; 03.75.Lm; 47.20.Ky; 05.45.Yv

I. INTRODUCTION

Solitons in two-dimensional (2D) settings have drawn a great deal of interest as they exhibit properties which are not available in 1D, such as vorticity, chirality, the possibility of the collapse and suppression of the collapse, spatial anisotropy, etc. In usual 2D systems, all localized modes supported by the ubiquitous cubic self-focusing nonlinearity are prone to instability driven by the critical collapse in the same setting [1–3]. 2D bright solitons with embedded vorticity are subject to an even stronger instability against perturbations breaking their axial symmetry [4]. Therefore, the creation of *stable* 2D, and even 3D, bright solitary waves and vortices remains a challenging problem, especially in the fields of optics and Bose-Einstein condensates, where the self-focusing cubic nonlinearity represents, respectively, the Kerr effect [5] and attractive interactions between atoms, which may be induced by the Feshbach resonance [6–8].

A general method to stabilize solitons in 2D geometry is provided by the use of spatially periodic potentials. In optics, such potentials can be imposed by virtual photonic lattices in photorefractive crystals [9], and permanent lattices written in bulk silica [10], while in BECs similar potentials can be induced by interference patterns (optical lattices) created by coherent laser beams illuminating the condensate [11]. Although the periodical potentials can provide diverse functionalities, they limits the mobility of solitons. To preserve the full mobility, stabilization of solitons in the 2D free space is a challenging objective. A possible way is suggested by using self-focusing nonlinearities weaker than cubic. Indeed, quadratic (alias second-harmonic generating) nonlinearity does not cause collapse in 2D [12–14]. However, the quadratic nonlinearity does not remove the azimuthal splitting instability of vortex solitons [15]. Another possibility is the use of competing cubic self-focusing and quintic self-defocusing nonlinear terms to stabilize 2D solitons [16–18]. In this setting, all the fundamental solitons are stable, while vortex solitons are stabilized above a specific threshold [19, 20], which was not, thus far, achieved in the experiment.

The most straightforward means to stabilize fundamental and vortical solitons in 2D free space is offered by the use of nonlocal nonlinearity. In particular, nonlocal nonlinear response in plasmas is induced by heating and ionization [21], and the propagation of light in nematic liquid crystals features nonlocality resulting from long-range molecular interactions [22]. In BECs, nonlocality originates from isotropic long-range Van der Waals interactions between

*Electronic address: yongyaoli@gmail.com

Rydberg atoms [23, 24], as well as from dipole-dipole interactions (DDIs) between atoms or molecules possessing permanent magnetic or electric dipole moments [25–31], or moments induced by an external polarizing field [32]. Permanent quadrupole moments give rise to similar long-range interactions in a molecular BEC [33]. The latter one, DDI, features strong tunability, which can be isotropic or anisotropic in the 2D plane by setting the dipoles perpendicular or parallel to the plane.

A completely different approach to the creation of self-trapped fundamental and vortex modes was proposed in Refs. [34–39]. It relies on the use of defocusing nonlinearity in the D-dimensional space, with the local strength growing from the center to periphery, as a function of radius r, at any rate faster than r^D. It has been shown that such setting can support extremely robust families of soliton and solitary vortices.

Recently, an unexpected result was revealed by the analysis of a two-component (spinor) self-attractive BEC with the linear spin-orbit (SO) coupling between the components, *viz.*, the prediction of completely stable 2D solitons of two types, namely, semi-vortices and mixed modes (MMs) [40–46]. The semi-vortices are built of one zero-vorticity and one vortical components, while the MMs mix zero and non zero vorticities in both components. These findings contradict the common belief that any system with the pure cubic self-focusing cannot support stable solitons in the free 2D space.

In comparison to the stabilization of 2D solitons in free space, a still more challenging objective is creation of stable *anisotropic* solitary vortices, i.e., bright anisotropic vortex solitons (AVSs). Obviously, the use anisotropic DDI, corresponding to the in-plane polarization of the atomic moments, is a natural way to achieve this purpose. However, stable AVSs supported solely by anisotropic DDIs have not been reported, thus far. On the other hand, recent consideration of the SO-coupled BEC in the free space, with nonlinearity represented by anisotropic DDIs, has predicted stable AVSs of the semi-vortex type [47]. Similar vortex modes were predicted as gap solitons in the simplified 2D free-space model, with kinetic terms dropped in comparison with the strong SO coupling [48]. In the latter case, the bandgap structure was induced, instead of lattice potentials, by the interplay of the SO coupling with the Zeeman splitting (ZS).

The anisotropy of these vortices manifests itself in deformation of their shapes. The AVS created in the full model (which includes the kinetic energy) features a 2D density profile resembling a slim peanut elongated parallel to the (in-plane) orientation of dipole moments in the condensates (we define it as axis x in the 2D plane, i.e., as the *horizontal direction*). In particular, the density profile of the vortex component features two symmetric maxima separated in the horizontal direction, see Fig.1(a2) in Ref. [47] and the top row in Fig. 1 displayed below. Therefore, we refer to AVS modes of this type as "horizontal" ones. On the other hand, the profile of AVSs found as the gap solitons is essentially "fatter" in the vertical direction, perpendicular to the in-plane orientation of the dipole moments, see Fig. 3(b1) in Ref. [48] and the second row in Fig. 1 below. In particular, the vortex component of the gap-soliton AVSs features two density maxima separated in the vertical direction. Accordingly, we call similarly shaped AVSs "vertical" ones. Moreover, these two types of AVSs have opposite signs of their effective dynamical mass, negative and positive, for the horizontal and vertical modes, respectively.

One objective of the present work is to figure out the reason for the difference between the horizontal and vertical AVSs, and find a way to control their shapes. Further, we aim to study mobility of the AVSs, and to elaborate a new species of *inverted* AVSs, which have their zero-vorticity and vortex constituents placed in the higher- and lower-energy components, as defined by the ZS. Our study is based on the model of the spinor BEC with the in-plane polarization of atomic moments, combining the linear SO coupling of the Rashba type, nonlinear long-range DDI, and the ZS effect.

The paper is structured as follows. The model is introduced in Section II. Basic numerical results for the horizontal and vertical AVSs, supported by some analytical considerations, are reported in Section III. The mobility problem for horizontal AVSs is considered, by means of systematic simulations, in Section IV. The novel type of inverted AVSs (of the horizontal type), which turn out to be excited states, in comparison with the ground states realized by the usual AVSs, and, quite surprisingly, are *stable* in a large parameter region, are addressed in Section V. The paper is concluded by Section VI.

II. THE MODEL

Under the mean-field approximation, the evolution of the spinor wave functions of the dipolar BECs, $\psi = (\psi_+, \psi_-)$, is governed by the coupled Gross-Pitaevskii equations, written here in the normalized form, which include the SO

coupling and ZS, with strength Ω:

$$i\partial_t\psi_+ = -\frac{1}{2}\nabla^2\psi_+ + \lambda\hat{D}^{[+]}\psi_- - \Omega\psi_+ + \psi_+\int d\mathbf{r}' R(\mathbf{r}-\mathbf{r}')(|\psi_+(\mathbf{r}')|^2 + |\psi_-(\mathbf{r}')|^2),$$
$$i\partial_t\psi_- = -\frac{1}{2}\nabla^2\psi_- - \lambda\hat{D}^{[-]}\psi_+ + \Omega\psi_- + \psi_-\int d\mathbf{r}' R(\mathbf{r}-\mathbf{r}')(|\psi_+(\mathbf{r}')|^2 + |\psi_-(\mathbf{r}')|^2). \quad (1)$$

Here operators of the SO-coupling are

$$\hat{D}^{[\pm]} = \partial_x \mp i\partial_y, \quad (2)$$

and its strength is fixed to be $\lambda \equiv 1$, by means of rescaling. The DDI's kernel is

$$R(\mathbf{r}-\mathbf{r}') = \frac{1-3\cos^2\theta}{(\epsilon^2+|\mathbf{r}-\mathbf{r}'|^2)^{3/2}}, \quad (3)$$

where cutoff ϵ is determined by the confinement in the transverse (third) dimension [48]. The form of this kernel implies that the dipoles are polarized (by an external magnetic field), as said above, in the positive x direction in 2D (x,y) plane, hence $\cos^2\theta \equiv (x-x')^2/|\mathbf{r}-\mathbf{r}'|^2$.

Stationary states are looked for as the usual form, $\psi_\pm(\mathbf{r},t) = \phi_\pm(\mathbf{r})e^{-i\mu t}$, where $\phi_\pm$ are stationary wave functions, and μ is a real chemical potential. A dynamical invariant of the system is the total norm, which is proportional to the total number of atoms in the binary BECs:

$$N = N_+ + N_- = \int d\mathbf{r}(|\phi_+|^2 + |\phi_-|^2). \quad (4)$$

It is also relevant to define the relative share of the total number of atoms which are kept in the vortex component:

$$F_- = N_-/\left(N_+ + N_-\right). \quad (5)$$

The other dynamical invariants are the linear momentum [see Eq. (15) below] and total energy,

$$E = E_{\rm K} + E_{\rm DDI} + E_{\rm SOC} + E_{\rm ZS}\ , \quad (6)$$

where $E_{\rm K}$, $E_{\rm DDI}$, $E_{\rm SOC}$ and $E_{\rm ZS}$ are the kinetic energy and the terms representing DDI, SO coupling and ZS, respectively:

$$E_{\rm K} = \frac{1}{2}\int d\mathbf{r}\left(|\nabla\phi_+|^2 + |\nabla\phi_-|^2\right),$$
$$E_{\rm DDI} = \frac{1}{2}\iint d\mathbf{r}d\mathbf{r}'\left(|\phi_+(\mathbf{r})|^2 + |\phi_-(\mathbf{r})|^2\right)R(\mathbf{r}-\mathbf{r}')(|\phi_+(\mathbf{r}')|^2 + |\phi_-(\mathbf{r}')|^2),$$
$$E_{\rm SOC} = \int d\mathbf{r}(\phi_+^*\hat{D}^{[+]}\phi_- - \phi_-^*\hat{D}^{[-]}\phi_+),$$
$$E_{\rm ZS} = -\int d\mathbf{r}\Omega(|\phi_+|^2 - |\phi_-|^2). \quad (7)$$

Note that the anisotropic system does not conserve the total orbital angular momentum, but its standard definition for each component,

$$\langle L_\pm\rangle = \frac{1}{N_\pm}\int \phi_\pm^*\hat{L}\phi_\pm d\mathbf{r}, \quad (8)$$

where $\hat{L} = -i(y\partial_x - x\partial_y)$ is the angular-momentum operator, can be used to characterize the degree of vorticity of the components.

Bright-soliton modes of the semi-vortex type in various systems may be produced by the simple input [40],

$$\phi_+^0 = A_+\exp(-\alpha_+ r^2), \quad \phi_-^0 = A_- r\exp(i\theta - \alpha_- r^2), \quad (9)$$

where $A_\pm$ and $\alpha_\pm$ are positive constants, ϕ_+ and ϕ_- being the zero-vorticity (fundamental) and vortex components, respectively. Starting from this input AVS can be produced by the imaginary-time-integration method [49–51]. In the following sections, we numerically identify different types of AVSs by varying two control parameters, *viz.*, the total norm of the soliton, as given by Eq. (4), and the ZS strength, i.e., Ω in Eq. (1).

Note that, fixing $\Omega > 0$ in Eq. (7), ansatz (9) implies that the fundamental and vortical components are lower-energy and higher-energy ones, respectively. The opposite situation, with $\Omega < 0$ (the inverted AVS) is possible too and is considered below in Section V.

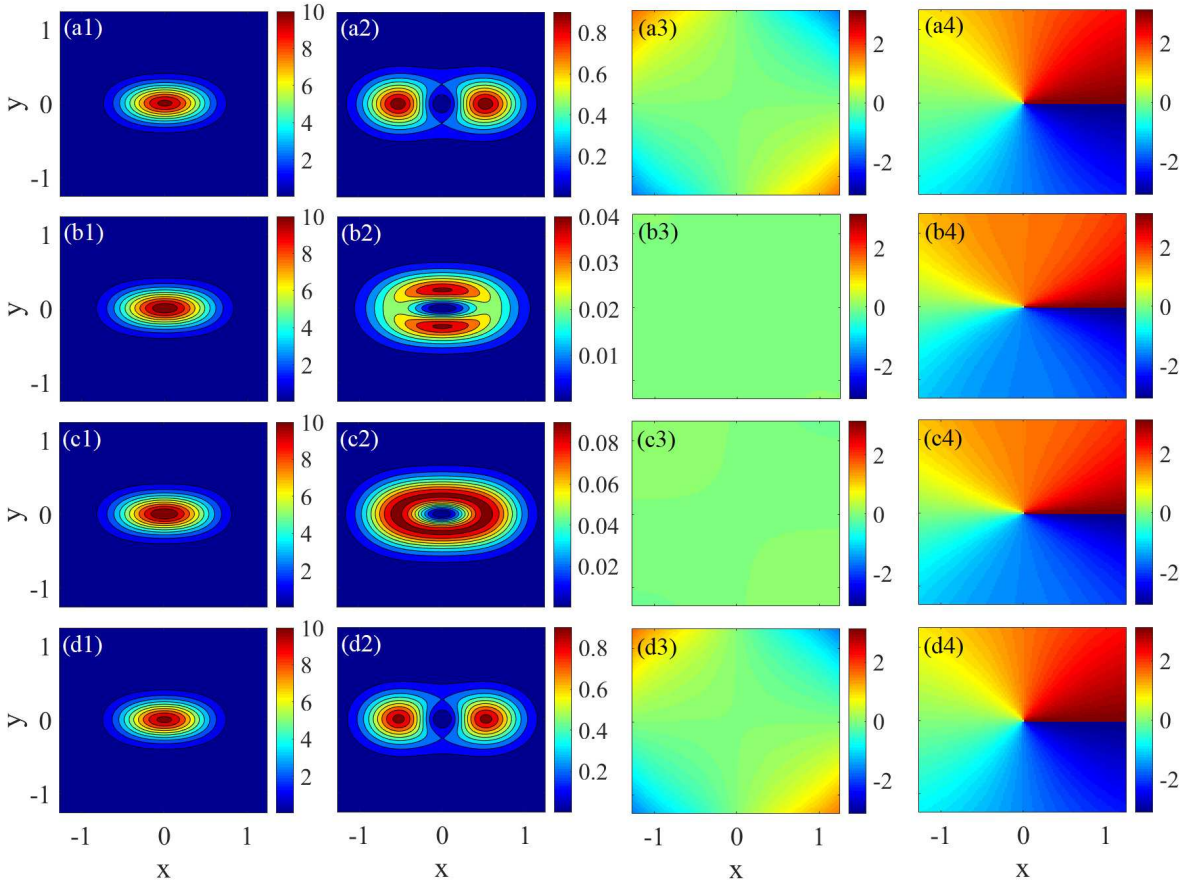

FIG. 1: Displayed in the first row (from left to right) are, severally, the density profiles of the fundamental and vortical components (ϕ_+ and ϕ_-, respectively), and their phase profiles, for $(N, \Omega) = (5, 0)$, which represents a typical horizontally oriented AVS. The second row: the same, but for $(N, \Omega) = (5, 10)$, providing an example of a vertical AVS. The third row: the same for $(N, \Omega) = (5, 4.23)$, which represents an AVS in the form of an elliptic ring. It is located precisely at the border between horizontal and vertical modes. The fourth row: the same for $(N, \Omega) = (5, 0.0262)$, which represents a horizontal AVS with the infinite dynamical mass (see Fig. 5 below).

III. NUMERICAL AND SOME ANALYTICAL RESULTS FOR ANISOTROPIC SEMI-VORTICES

The first and the second rows of Fig. 1 display typical examples of horizontal and vertical AVSs with equal norms, generated by means of the imaginary-time simulations at different values of the ZS strength, Ω, starting from the same input (9). The results demonstrate that the horizontal mode is converted into its vertical counterpart, following the variation of Ω. At $\Omega \to 0$, it is the horizontal AVS, similar to those found in Ref. [47], while, at $\Omega > \Omega_{\rm C}$, it is transformed into a vertical one. To identify the respective critical value, $\Omega_{\rm C}$, we define a shape parameter,

$$\triangle = \frac{|\phi_-^{\max}(x,0)|^2 - |\phi_-^{\max}(0,y)|^2}{|\phi_-^{\max}(x,0)|^2 + |\phi_-^{\max}(0,y)|^2}, \tag{10}$$

where $|\phi_-^{\max}(x,0)|^2$ and $|\phi_-^{\max}(0,y)|^2$ are local density maxima of the vortex component along the x and y axis, respectively, Obviously, $\triangle > 0$ and $\triangle < 0$ correspond to the horizontal and vertical shape, respectively, $\Omega_{\rm C}$ being defined by $\triangle \equiv 0$. Figure 2(a) displays $\triangle$ as a function of Ω for different values of the total norm, N, which clearly shows the transition from the horizontal to vertical shape with the increase of Ω. Figure 2(b) shows the critical value, $\Omega_{\rm C}$, as a function of N. This dependence may be phenomenologically fitted by

$$\Omega_{\rm C} = 0.95N - 0.5 \tag{11}$$

for $N > 2$. When $N < 2$, $\Omega_{\rm C}$ deviates from this linear fit, approaching $\Omega_{\rm C} = 0.5$ at the limit of $N = 0$. The shape of the AVS precisely at $\Omega = \Omega_{\rm C}$ is displayed in the third row of Fig. 1, for $N = 5$. The density pattern of the vortex

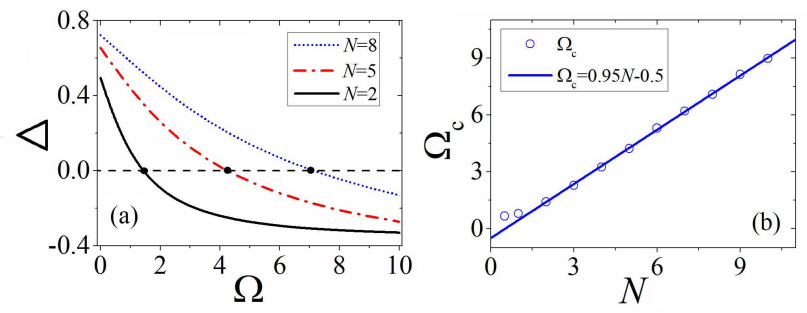

FIG. 2: (a) The shape parameter, $\triangle$, defined as per Eq. (10), vs. the Zeeman-splitting strength, Ω, for the total norm $N = 2$, 5, and 8 (black solid, red dashed-dotted, and blue dotted curves, respectively). Black circular dots designate critical values for the horizontal-vertical transition, $\Omega_{\rm C}(N)$. (b) $\Omega_{\rm C}$ vs. N; this dependence can be fitted by $\Omega_{\rm C} = 0.95N - 0.5$ for $N > 2$.

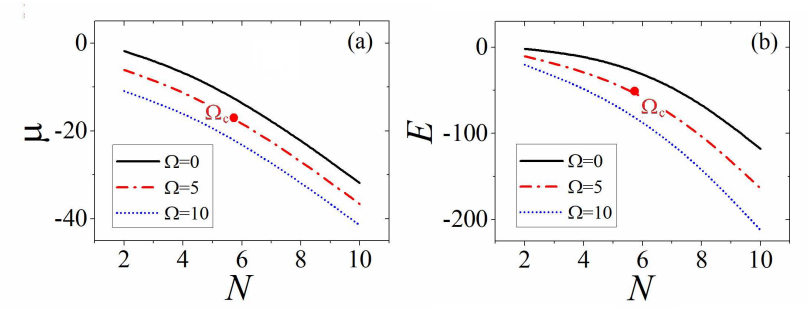

FIG. 3: (a) The chemical potential, μ, and (b) the energy, E [calculated as per Eq. (7)], vs. the total norm, N, for the numerically found AVS families at different values of the Zeeman-splitting strength, Ω. The two red circle dots on the red curves, i.e., $(N, \mu) = (5.78, -17.02)$ and $(N, E) = (5.78, -50.9)$, designate the location $\Omega_{\rm C}$, i.e., the boundary between the horizontal and vertical types of the AVS.

component (ϕ_-) of this semi-vortex mode features an elliptical ring with a nearly constant maximum value along it, hence it indeed may not be identified as a horizontal or vertical mode.

The horizontal-vertical shape transition of the vortex component, and, furthermore, the linear dependence between $\Omega_{\rm C}$ and N for large values of Ω and N may be qualitatively explained. Indeed, in the limit of large Ω (strong ZS), there is a larger term, $-\Omega$, in the condensate's chemical potential, hence solutions to Eq. (1) are looked for as

$$\psi_{\pm}(x, y, t) = e^{i\Omega t}\Psi_{\pm}(x, y, t), \tag{12}$$

where $\Psi_{\pm}$ are slowly varying functions, in comparison with $\exp(i\Omega t)$. Then, in the lowest approximation in small parameter $1/\Omega$, the substitution of expressions (12) in Eq. (1) leads to (cf. a similar approximation for different models with the SO-coupling, developed in Ref. [41])

$$i\partial_t \Psi_+ = -\left(\frac{1}{2} - \frac{\lambda^2}{4\Omega^2}\right)\nabla^2\Psi_+ + \Psi_+ \int d\mathbf{r}' R(\mathbf{r} - \mathbf{r}')(|\Psi_+(\mathbf{r}')|^2 + |\Psi_-(\mathbf{r}')|^2), \tag{13}$$

$$\Psi_- \approx (\lambda/2\Omega)\,\hat{D}^{[-]}\Psi_+ \,. \tag{14}$$

These results also imply that, at large Ω, the share of the norm in the vortex component, defined in Eq. (5), obeys scaling $F_- \sim \Omega^{-2}$, which is confirmed by the numerically found dependences $F_-(\Omega)$ displayed below in Fig. 8(a).

Thus, in the limit of large Ω, Eq. (13) is tantamount to the GPE for the single component (Ψ_+) in the dipolar condensate, which gave rise to stable anisotropic zero-vorticity solitons in Ref. [28], while the wave function of Ψ_- is essentially determined by Eq. (14). In particular, the shape of the soliton is, naturally, stretched along the horizontal direction, to minimize the DDI energy (making it negative for dipoles placed along a straight line, parallel to their orientation). Further, looking at the stretched shape of the ψ_+ component, in the second row of Fig. 1, it is obvious that it has the largest gradient, and, consequently, maxima of the field induced according to Eqs. (14) and (2), precisely at the vertical positions at which the density maxima of the ψ_- component are observed in the figure. On the other hand, if Ω is not too large, the ψ_- component keeps its nonlinearity (as its norm is not very small), and

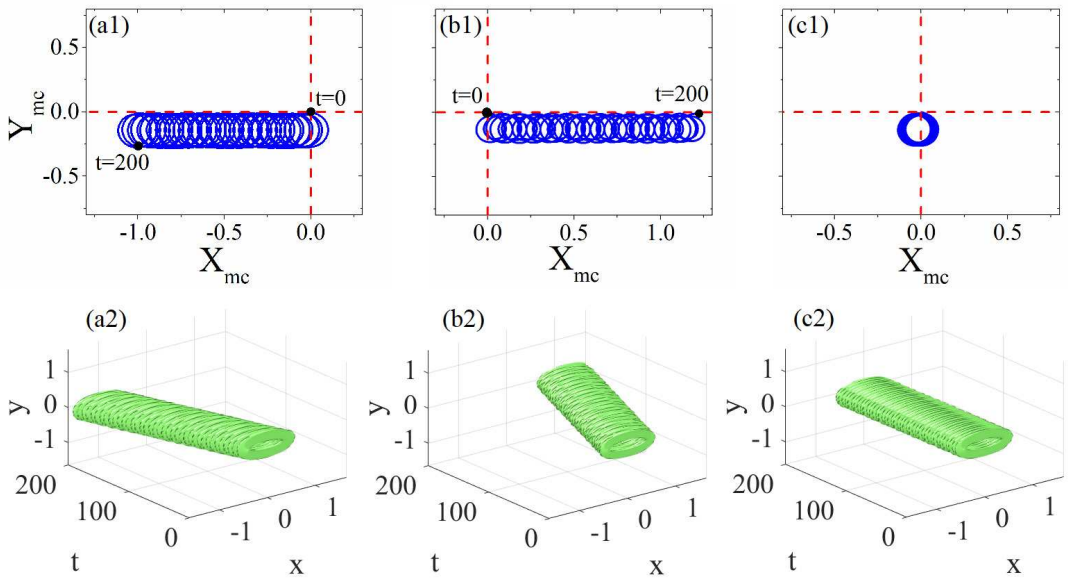

FIG. 4: Typical examples of motion of horizontal AVSs with negative ($\Omega = 0$) (a1,a2), positive ($\Omega = 0.06$) (b1,b2), and infinite ($\Omega = 0.0262$) effective mass (c1,c2) initiated by a horizontal kick, $\eta = 0.2$. The first row: trajectories of motion of the c.m. of the fundamental component, ϕ_+. The second row: isosurfaces of $|\phi_+|^2$. The total norm of the solitons in these panels is $N = 5$.

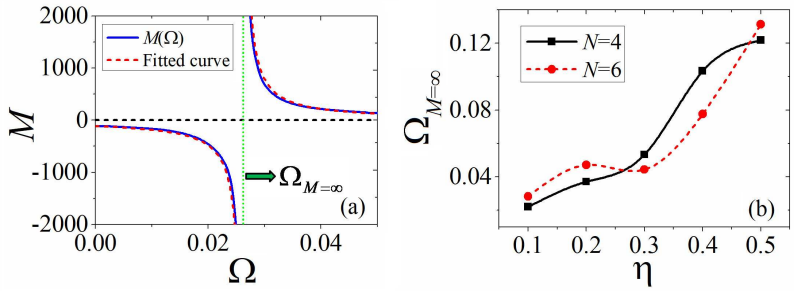

FIG. 5: (a) The effective mass of the AVSs vs. Ω for norm $N = 5$ and fixed initial kick $\eta = 0.2$. The mass diverges at $\Omega = \Omega_{M=\infty} = 0.0262$. Dependence $M(\Omega)$ is virtually exactly fitted by $3/(\Omega - \Omega_{M=\infty})$ (the red dash curve). (b) $\Omega_{M=\infty}$ vs. η for two values of norm N of the AVS. When $\Omega = 0$, the effective mass of the soliton is $M = -106.6$.

the minimization of the energy of the dipole-dipole interaction between the moments concentrated at density maxima of ψ_- obviously favors the horizontal shape, which is observed in the first row of Fig. 1. Finally, to estimate the critical value of Ω at the horizontal-vertical shape-transition point, we note that the transition is determined by the competition of the DDI and ZS energies. Looking at the respective terms in Eq. (7), it is easy to see that, in the limit of large Ω and large N, these energy scale as N^2 and ΩN, respectively, which explains that the transition must take place at $\Omega_C = \text{const} \cdot N$, in agreement with Eq. (11).

Finally, overall characteristics of the families of AVSs, produced by the numerical calculations, are provided by dependences of their chemical potential (μ) and total energy (E) on the total norm (N), which are displayed, for different fixed values of the ZS strength (Ω), in Figs. 3(a) and (b), respectively. In particular, it is worthy to note that the $\mu(N)$ curves always satisfy the the Vakhitov-Kolokolov criterion, $d\mu/dN < 0$, which is a well-known necessary stability condition for any soliton family supported by attractive interactions [1, 3, 52]. Because the dominant component, ϕ_+, occupies the lower energy level split by the Zeeman effect, and its share in the total norm grows with Ω, as shown by Eq. (14), it is easy to understand why both μ and E monotonously decrease with the increase of Ω. Finally, we stress that *all* the solitons are found to be stable for $\Omega > 0$.

IV. MOBILITY OF THE ANISOTROPIC SEMI-VORTICES

Mobility of the solitons in the system under the consideration is a nontrivial issue, as the presence of the SO-coupling terms in Eq. (1) breaks its Galilean invariance [40], although it conserve the total linear momentum (unlike the nonexisting angular momentum, as mentioned above):

$$\mathbf{P} = i \int d\mathbf{r} \left[(\nabla \psi_+^*) \psi_+ + (\nabla \psi_-^*) \psi_- \right]. \tag{15}$$

The mobility was tested in direct simulations by applying kick η to a stable quiescent AVS, $\phi_\pm(x,y)$, in the x or y direction. This correspond to simulating Eq. (1) with input

$$\psi_\pm(\mathbf{r}, t=0) = \phi_\pm(\mathbf{r}) \{e^{i\eta x}, e^{i\eta y}\}, \tag{16}$$

the respective components of momentum (15) being $P_{x,y} = N\eta$. The mobility is characterized by the effective masses for the motion of the soliton in the x and y, directions, defined as $M_{x,y} = P_{x,y}/V_{x,y}$, where $V_{x,y}$ are velocities of the AVSs in the x and y directions, respectively, produced in the simulations by the initial kick.

To define the trajectory of the kicked soliton, we introduce time-dependent coordinates of the c.m. (center-of-mass) of its fundamental component:

$$\{X_{\rm mc}(t), Y_{\rm mc}(t)\} = \frac{\int\int \{x,y\} |\psi_+(x,y,t)|^2 dxdy}{\int\int |\psi_+(x,y,t)|^2 dxdy}. \tag{17}$$

Indeed, the location of the c.m. of the entire two-component soliton is dominated by the fundamental component, as the vortical one carries a small share of the total norm, see Refs. [47, 48] and Fig. 8(a). The actual mobility of the kicked solitons was studied through the shape of the c.m. trajectories, at different values of Ω, as produced by real-time simulations of Eq. (1).

In this work, we consider only the motion induced by the kick applied in the horizontal (x) direction to the horizontal AVSs. Figures 4(a,b) illustrate the mobility of AVSs with $\Omega = 0$ and 0.06, initiated by the kick value $\eta = +0.2$. It is seen that the resulting spiral motion may be considered as a permanent drift of a circular trajectory of a small radius in either negative or positive direction of x. The circular component of the motion may be explained by the action of an effective Lorentz-like force, which is a manifestation of *macroscopic* SO coupling of the AVS's intrinsic vorticity to its progressive motion [53], although accurate consideration of this feature makes an additional detailed analysis necessary. Lastly, it is relevant to stress the two components of the AVS stay rigidly bound in the course of the motion.

The effective mass corresponding to the application of the kick along the x direction, $M(\Omega)$, is plotted as a function of Ω in Fig. 5(a). The figure reveals a surprising feature: with the increase of Ω, the effective mass changes its sign from negative to positive via *divergence* at a particular value of the ZS strength, $\Omega = \Omega_{M=\infty}$. The red fitting curve in Fig. 5(a) demonstrates that the effective mass diverges $\sim (\Omega - \Omega_{M=\infty})^{-1}$ at Ω close to $\Omega_{M=\infty}$. Figure 4(c) showing a typical example of real-time evolution of AVSs with $\Omega = \Omega_{M=\infty}$ kicked by $\eta = 0.2$. In this case, the direct simulations demonstrate, in Figs. 4(c1,c2), that the kicked vortex performs circular motion without any progressive drift, which may be construed as the effective immobility of the AVS.

The value of $\Omega_{M=\infty}$ depends on the total norm, as well as of the size η of the initial kick. This dependence is illustrated in Fig. 5(b) by means of curves of $\Omega_{M=\infty}(\eta)$ for two fixed values of N, which show that $\Omega_{M=\infty}$ increases with the growth of η. It is worthy to note that the essential dependence of the effective mass on the ZS strength occurs at quite small values of Ω, therefore all the relevant AVSs are of the horizontal type [the transition to the vertical shape happens at much higher values of Ω, see Fig. 2(b)]. It follows from here that all the AVSs of the vertical type have the positive effective mass. This conclusion explains why the horizontal AVSs in Ref. [47], and vertical ones in Ref. [48] feature opposite signs of their dynamical mass, as mentioned above. Finally, the numerical results demonstrate that the effective mass approaches the norm of the soliton, i.e., $M \to N$ in the limit of $\Omega \to \infty$. This conclusion is easily explained by the fact that, in the limit of $\Omega \to \infty$, the AVS turns into a usual single-component soliton [see Eq. (14)], whose dynamical mass is always identical to N.

V. INVERTED ANISOTROPIC SEMI-VORTICES, WITH $\Omega < 0$

As stressed above, we considered the soliton modes of semi-vortex type, with their fundamental and vortex constituents sitting, respectively, in lower- and higher-energy components, in terms of the ZS with $\Omega > 0$. Here, we aim to consider the reverse setting, with $\Omega < 0$, when the fundamental and vortex parts find themselves in the higher-

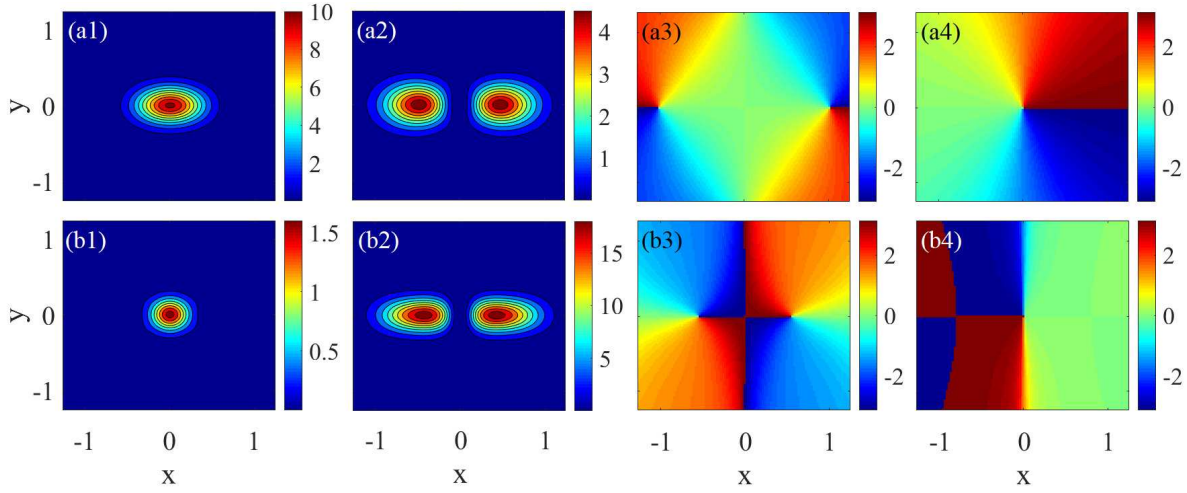

FIG. 6: The same as in Fig. 1, but for the inverted AVSs, with $\Omega < 0$. The first row represents a stable AVS with $(N, \Omega) = (6, -1.82)$, with equal norms in the fundamental and vortex components. The second row shows the soliton with $(N, \Omega) = (10, -10.8)$, which is a dipole mode for ϕ_- and located at the stability boundary [see Fig. 8(a) below].

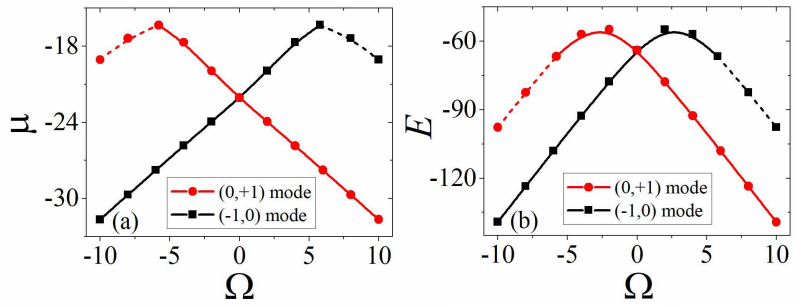

FIG. 7: The chemical potentials (a) and energy (b) for the mode under the consideration, with vorticities in the ψ_+ and ψ_- components $(S_+, S_-) = (0, +1)$, and its flipped counterpart, with $(S_+, S_-) = (-1, 0)$, with a fixed norm, $N = 8$, vs. the Zeeman-splitting strength, Ω.

and lower-energy components, respectively. Because the fundamental constituents tends to carry a much larger share of the total norm than its vortical counterpart, one may expect that the inverted state will be an excited one, while the stable states considered above were ground states in the system. For this reason, it is quite interesting to explore the shape and, especially, stability of these excited states. Surprisingly, it is found below that they are stable in a considerable part of their parameter space.

Generic examples of the density and phase structure of the inverted AVSs are displayed in Fig. 6. As well as these examples, all the inverted AVSs feature the horizontal structure, as it is defined above (with two density maxima separated along the x axis, i.e., along the direction of the polarization of dipoles in the underlying condensate). Unlike the case of large positive Ω considered above, vertical inverted AVSs have not been found.

The dependence of the AVS's chemical potential and energy on Ω at fixed norm N is displayed in Fig. 7, both for the mode under the consideration, and its *flipped* counterpart, with vorticities -1 and 0 in components ψ_+ and ψ_-, respectively. In the absence of the ZS, $\Omega = 0$, both semi-vortex modes are fully equivalent to each other [40]. Further, the present mode at given Ω and the flipped one at the ZS strength $-\Omega$ remain equivalent too. Thus, Fig. 7(b) makes it obvious that the present mode is an excited state at $\Omega < 0$, as its energy is higher than the energy of the ground state, which is realized, at $\Omega < 0$, by the flipped AVS mode.

Further, Fig. 8(a) represents families of the AVS modes by displaying the share of the norm in the vortex component, F_-, defined according to Eq. (5), vs. Ω at several fixed values of N. Naturally, F_- increases with the growth of $-\Omega$. A nontrivial finding is that, although the inverted AVS is an excited state, as shown above, it has a vast stability region, $\Omega > \Omega_{\rm s}(N)$, with the dependence of the stability boundary on N, i.e., $\Omega_{\rm s}(N)$, shown in Fig. 8(c). In particular, Fig. 8(a) demonstrates that, at $N > 2$, the AVS stabilizes itself by shifting more than half of the total norm to the lower-energy vortex component, making it a dominant one in the semi-vortex soliton. In previously studied models,

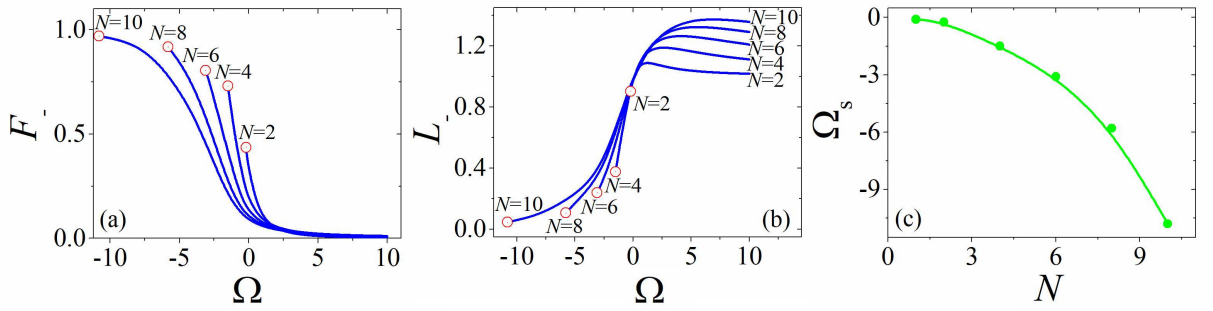

FIG. 8: (a) The share of the total norm in the vortex component [see Eq. (5)], $F_{-}(\Omega)$, as a function of the Zeeman-splitting strength, Ω, at fixed values of the total norm, N. (b) The angular momentum of the vortex component, defined as per Eq. (8), vs. Ω, at fixed values of N. In both panels (a) and (b), stable branches are shown by blue solid curves. Red circles at the end of the blue curves designate the stability boundary, $\Omega = \Omega_{\rm s}(N)$. The inverted modes (corresponding to $\Omega < 0$) exist too at $\Omega < \Omega_{\rm s}(N)$, but are unstable in that region. (c) The stability boundary, $\Omega_{\rm s}$, as a function of N.

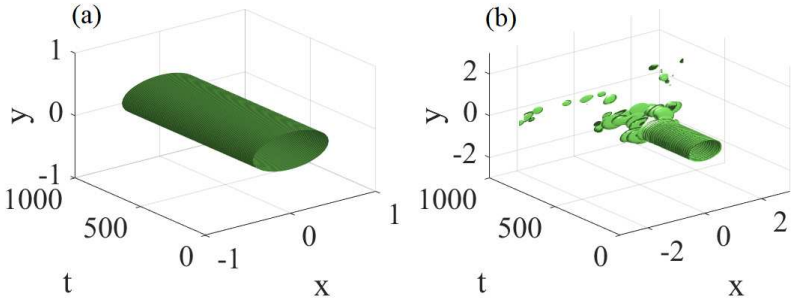

FIG. 9: Plots of $|\phi_{+}(x,y,t)|^2$ depict evolution of typical examples of stable (a) and unstable (b) inverted AVSs, for $(N,\Omega) = (5,-1.5)$ and $(5,-2.4)$, respectively. For this value of the total norm, $N = 5$, the stability boundary is $\Omega_{\rm s} = -2.2$, see Fig. 8(c).

stable SVs with a dominant vortex component were never found [40, 41, 45, 47, 48]. In fact, previous studies have never produced *stable* excited states of SVs either (unstable excited states were found in some cases [40, 45]).

As the vortex mode becomes dominant with the increase of $-\Omega$ (still remaining stable), its shape actually becomes "less vortical", as may be quantified by the dependence of its angular momentum, which is calculated pursuant to Eq. (8) and displayed, as a function of Ω, in Fig. 8(b). The plots displayed in the second row of Fig. 6 suggest that the trend to the loss of the angular momentum with the growth of $-\Omega$ (at fixed N) may be explained by gradual evolution of the dominant component toward a dipole mode [See in the second row of Fig. 6], while keeping the vorticity.

Typical examples of a stable and unstable inverted AVSs, which are selected, respectively, from intervals $\Omega > \Omega_{\rm s}$ and $\Omega < \Omega_{\rm s}$ for the same N, are displayed in Fig. 9. The unstable mode suffers spontaneous fragmentation after stably propagating for a while.

VI. CONCLUSION

The objective of this work is to study anisotropic vortex solitons (AVSs) in dipolar SO (spin-orbit)-coupling BECs, controlled by the strength of the ZS (Zeeman splitting). The dipolar condensate was considered in the strongly anisotropic form, with the in-plane polarization of the atomic dipoles. This setting, although being relatively complex, makes it possible to construct stable anisotropic vortices [in fact, *semi-vortices* (SVs), i.e., bound states of zero-vorticity and vorticity-1 components], which was not possible in previously studied systems.

Here, we have demonstrated that the shape and stability of the AVSs are efficiently controlled by the ZS strength, Ω. In the case of $\Omega > 0$, which corresponds to the AVS's fundamental and vortex constituents placed, respectively, in the lower- and higher-energy components, as defined by the ZS, the increase of Ω leads to the transition from the horizontal to vertical shape of the AVS, the horizontal direction being the one aligned with the atomic dipole moments. The value of Ω at the horizontal-vertical transition, $\Omega_{\rm C}$, was found in the numerical form, and its nearly linear dependence on the total norm, N, was explained. Exactly at $\Omega = \Omega_C$, the AVS assumes an elliptic-ring shape.

Mobility of the AVSs was studied too, by means of direct simulations of initially kicked solitons. As a result, they exhibit circular motion with a small radius, with a systematic drift in the direction of the kick or *against* it. It was found that the AVS's effective mass is *negative* in an interval of $0 < \Omega < \Omega_{M=\infty}$, and positive at $\Omega > \Omega_{M=\infty}$. The effective mass changes its sign at $\Omega = \Omega_{M=\infty}$ via the divergence, as $M_{\rm eff} \sim (\Omega - \Omega_{M=\infty})^{-1}$.

Unexpected results have been reported for the *inverted* AVSs, i.e., ones at $\Omega < 0$, with the fundamental and vortex constituents placed by the ZS in the higher- and lower-energy components, respectively. The inverted AVS is always an excited state (with a horizontal structure), which coexists with a lower-energy ground state (horizontal or vertical one). A surprising result is that these excited states are stable in a large parameter region. In previously studied SO-coupled nonlinear systems, excited were always unstable.

The present analysis can be extended in some directions. First, a natural possibility is to simulate collisions between mobile AVSs. Next, one can consider the limit case of strong SO coupling and strong ZS, when the kinetic-energy terms may be neglected in Eq. (1), which gives rise to the bandgap spectrum [48]. It may be interesting to construct AVSs of the gap-soliton type, that may populated the bandgap. On the other hand, it may be interesting too to consider the ZS with a time-dependent strength and the respective "management" regimes for AVSs. Finally, a challenging option is to seek extension of current setting to the 3D geometry.

Acknowledgments

This work was supported, in part, by NNSFC (China) through Grant No. 11575063, 61471123, 61575041, by the joint program in physics between NSF and Binational (US-Israel) Science Foundation through project No. 2015616, and by the Natural Science Foundation of Guangdong Province, through Grant No. 2015A030313639. B.A.M. appreciates a foreign-expert grant of the Guangdong province (China).

[1] L. Bergé, Wave collapse in physics: principles and applications to light and plasma waves, Phys. Rep. **303**, 259 (1998).
[2] G. Fibich and G. Papanicolaou, Self-focusing in the perturbed and unperturbed nonlinear Schrödinger equation in critical dimension, SIAM J. Appl. Math. **60**, 183 (1999).
[3] G. Fibich, The Nonlinear Schrödinger Equation: Singular Solutions and Optical Collapse (Springer: Cham, 2015).
[4] A. S. Desyatnikov, L. Torner, and Y. S. Kivshar, Optical vortices and vortex solitons, Prog. Opt. **47**, 1 (2005).
[5] Y. S. Kivshar and G. P. Agrawal,Optical Solitons: From Fibers to Photonic Crystals (Academic Press, San Diego, 2003).
[6] S. E. Pollack, D. Dries, M. Junker, Y. P. Chen, T. A. Corcovilos, and R. G. Hulet, Extreme Tunability of Interactions in a ^{7}Li Bose-Einstein Condensate, Phys. Rev. Lett. **102**, 090402 (2009).
[7] D. M. Bauer, M. Lettner, C. Vo, G. Rempe, and S. Dürr, Control of a magnetic Feshbach resonance with laser light, Nat. Phys. **5**, 339 (2009).
[8] M. Yan, B. J. DeSalvo, B. Ramachandhran, H. Pu, and T. C. Killian, Controlling Condensate Collapse and Expansion with an Optical Feshbach Resonance, Phys. Rev. Lett. **110**, 123201 (2013).
[9] N. K. Efremidis, S. Sears, D. N. Christodoulides, J. W. Fleischer, and M. Segev, Discrete solitons in photorefractive optically induced photonic lattices, Phys. Rev. E **66**, 046602 (2002).
[10] A. Szameit, J. Burghoff, T. Pertsch, S. Nolte, A. Tünnermann, and F. Lederer, Two-dimensional soliton in cubic fs laser written waveguide arrays in fused silica, Opt. Express **14**, 6055 (2006).
[11] O. Morsch and N. Oberthaler, Dynamics of Bose-Einstein condensates in optical lattices, Rev. Mod. Phys. **78**, 179 (2006).
[12] A. A. Kanashov and A. M. Rubenchik, On diffraction and dispersion effect on 3-wave interaction, Physica D **4**, 122 (1981).
[13] B. A. Malomed, P. Drummond, H. He, A. Berntson, D. Anderson, and M. Lisak, Spatio-temporal solitons in optical media with a quadratic nonlinearity, Phys. Rev. E **56**, 4725 (1997).
[14] X. Liu, K. Beckwitt, and F. Wise, Two-dimensional optical spatiotemporal solitons in quadratic media, Phys. Rev. E **62**, 1328 (2000).
[15] W. J. Firth, and D. V. Skryabin, Optical Solitons Carrying Orbital Angular Momentum, Phys. Rev. Lett. **79**, 2450 (1997).
[16] K. Dimitrevski, E. Reimhult, E. Svensson, A. Öhgren, D. Anderson, A. Berntson, M. Lisak, and M. L. Quiroga-Teixeiro, Analysis of stable self-trapping of laser beams in cubic-quintic nonlinear media, Phys. Lett. A **248**, 369 (1998).
[17] M. L. Quiroga-Teixeiro, A. Berntson, and H. Michinel, Internal dynamics of nonlinear beams in their ground states: short- and long-lived excitation, J. Opt. Soc. Am. B **16**, 1697-1704 (1999).
[18] D. Mihalache, D. Mazilu, F. Lederer, Y. V. Kartashov, L.-C. Crasovan, L. Torner, and B. A. Malomed. Stable vortex tori in the three-dimensional cubic-quintic Ginzburg-Landau equation. Phys. Rev. Lett. **97**, 073904 (2006).
[19] M. Quiroga-Teixeiro and H. Michinel, Stable azimuthal stationary state in quintic nonlinear optical media, J. Opt. Soc. Am. B **14**, 2004-2009 (1997).
[20] R. L. Pego and H. A. Warchall, Spectrally stable encapsulated vortices for nonlinear Schrödinger equations, J. Nonlin. Sci. **12**, 347-394 (2002).

[21] A. G. Litvak, V. A. Mironov, G. M. Fraiman, and A. D. Yunakovskii, Thermal self-effect of wave beams in a plasma with a nonlocal nonlinearity, Sov. J. Plasma Phys. **1**, 31 (1975).

[22] M. Peccianti, C. Conti, G. Assanto, A. De Luca, and C. Umeton, Routing of anisotropic spatial solitons and modulational instability in liquid crystals, Nature **432**, 733 (2004).

[23] R. Heidemann, U. Raitzsch, V. Bendkowsky, B. Butscher, W. R. Löw, and T. Pfau, Rydberg excitation of Bose-Einstein condensates, Phys. Rev. Lett. **100**, 033601 (2008).

[24] F. Maucher, N. Henkel, M. Saffman, W. Królikowski, S. Skupin, and T. Pohl, Rydberg-Induced Solitons: Three-Dimensional Self-Trapping of Matter Waves, Phys. Rev. Lett. **106**, 170401 (2011).

[25] T. Lahaye, C. Menotti, L. Santos, M. Lewenstein, and T. Pfau, The physics of dipolar bosonic quantum gases, Rep. Prog. Phys. **72**, 126401 (2009).

[26] P. Pedri and L. Santos, Two-dimensional bright solitons in dipolar Bose-Einstein Condensates, Phys. Rev. Lett. **95**, 200404 (2005).

[27] R. Nath, P. Pedri, and L. Santos, Stability of Dark Solitons in Three Dimensional Dipolar Bose-Einstein Condensates, Phys. Rev. Lett. **101**, 210402 (2008).

[28] I. Tikhonenkov, B. A. Malomed, and A. Vardi, Anisotropic Solitons in Dipolar Bose-Einstein Condensates, Phys. Rev. Lett. **100**, 090406 (2008).

[29] I. Tikhonenkov, B. A. Malomed, and A. Vardi, Vortex solitons in dipolar Bose-Einstein condensates, Phys. Rev. A **78**, 043614 (2008).

[30] M. Raghunandan, C. Mishra, K. Lakomy, P. Pedri, L. Santos, and R. Nath, Two-dimensional bright solitons in dipolar Bose Einstein condensates with tilted dipoles, Phys. Rev. A **92**, 013637 (2015).

[31] J. Huang, X. Jiang, H. Chen, Z. Fan, W. Pang, Y. Li, Quadrupolar matter-wave soliton in two-dimensional free space, Front. Phys. **10**, 100507 (2015).

[32] Y. Li, J. Liu, W. Pang, and B. A. Malomed, Matter-wave solitons supported by field-induced dipole-dipole repulsion with a spatially modulated strength, Phys. Rev. A **88**, 053630 (2013).

[33] Y. Li, J. Liu, W. Pang, and B. A. Malomed, Lattice solitons with quadrupolar intersite interactions, Phys. Rev. A **88**, 063635 (2013).

[34] O. V. Borovkova, Y. V. Kartashov, B. A. Malomed,and L. Torner, Algebraic bright and vortex solitons in defocusing media, Opt. Lett. **36**, 3088 (2011).

[35] O. V. Borovkova, Y. V. Kartashov, L. Torner, and B. A. Malomed, Bright solitons from defocusing nonlinearities, Phys. Rev. E **84**, 035602 (2011).

[36] R. Driben, Y. V. Kartashov, B. A. Malomed, T. Meier, and L. Torner, Soliton Gyroscopes in Media with Spatially Growing Repulsive Nonlinearity, Phys. Rev. Lett. **112**, 020404 (2014).

[37] Q. Tian, L. Wu, Y. Zhang, and J.-F. Zhang, Vortex solitons in defocusing media with spatially inhomogeneous nonlinearity, Phys. Rev. E **85**, 056603 (2012).

[38] Y. Wu, Q. Xie, H. Zhong, L. Wen, and W. Hai, Algebraic bright and vortex solitons in self-defocusing media with spatially inhomogeneous nonlinearity, Phys. Rev. A **87**, 055801 (2013).

[39] Y. V. Kartashov, B. A. Malomed, Y. Shnir, and L. Torner, Twisted Toroidal Vortex-Solitons in Inhomogeneous Media with Repulsive Nonlinearity, Phys. Rev. Lett. **113**, 264101 (2014).

[40] H. Sakaguchi, B. Li, B. A. Malomed, Creation of two-dimensional composite solitons in spin-orbit-coupled self-attractive Bose-Einstein condensates in free space, Phys. Rev. E **89**, 032920 (2014).

[41] H. Sakaguchi, E. Y. Sherman, and B. A. Malomed, Vortex solitons in two-dimensional spin-orbit coupled Bose-Einstein condensates: Effects of the Rashba-Dresselhaus coupling and Zeeman splitting, Phys. Rev. E **90**, 032202(2016).

[42] S. Gautam and S. K. Adhikari, Vortex-bright solitons in a spin-orbit-coupled spin-1 condensate, Phys. Rev. A **95**, 013608 (2017).

[43] G. Chen, Y. Liu, H. Wang, Mixed-mode solitons in quadrupolar BECs with spin-orbit coupling, Commun. Nonlinear Sci. Numer. Simulat. **48**, 318 (2017).

[44] Y. Zhang, Z. Zhou, B. A. Malomed, and H. Pu, Stable Solitons in Three Dimensional Free Space without the Ground State: Self-Trapped Bose-Einstein Condensates with Spin-Orbit Coupling, Phys. Rev. Lett. **115**, 253902 (2015).

[45] Y. Li, Z. Luo, Y. Liu, Z. Chen, C. Huang, S. Fu, H. Tan, and B. A. Malomed, Two-dimensional solitons and quantum droplets supported by competing self- and cross-interactions in spin-orbit-coupled condensates, ePrint arXiv:1706.06725 (2017).

[46] Y. Zhang, M. E. Mossman, T. Busch, P. Engels, C. Zhang, Properties of spin-orbit-coupled Bose-Einstein condensates, Front. Phys. **11**, 118103 (2016).

[47] X. Jiang, Z. Fan, Z. Chen, W. Pang, Y. Li, and B. A. Malomed, Two-dimensional solitons in dipolar Bose-Einstein condensates with spin-orbit coupling, **93**, 023633 (2016).

[48] Y. Li, Y. Liu, Z. Fan, W. Pang, S. Fu, and B. A. Malomed, Two-dimensional dipolar gap solitons in free space with spin-orbit coupling, Phys. Rev. A. **95**, 063613 (2017).

[49] L. M. Chiofalo, S. Succi,and P. M. Tosi, Ground state of trapped interacting Bose-Einstein condensates by an explicit imaginary time algorithm, Phys. Rev. E **62**, 7438 (2000).

[50] J. Yang and T. I. Lakoba, Accelerated imaginary-time evolution methods for the computation of solitary waves, Stud. Appl. Math. **120**, 265 (2008).

[51] J. Yang, and T. I. Lakoba, Universally-convergent squared-operator iteration methods for solitary waves in general nonlinear wave equations, Stud. Appl. Math. **118**, 153 (2007).

[52] M. Vakhitov and A. Kolokolov, Stationary solutions of the wave equation in a medium with nonlinearity saturation,

Radiophys. Quantum Electron. **16**, 783 (1973).
[53] L. Wen, Q. Sun, Y. Chen, D.-S. Wang, J. Hu, H. Chen, W.-M. Liu, G. Juzeliūnas, B. A. Malomed, and A.-C. Ji, Motion of solitons in one-dimensional spin-orbit-coupled Bose-Einstein condensates, Phys. Rev. A **94**, 061602(R) (2016)